metals

MDPI

Article

Influence of the Applied External Magnetic Field on the Deposition of Ni–Cu Alloys

Katarzyna Skibińska [1,*], Safya Elsharkawy [1,2], Karolina Kołczyk-Siedlecka [1], Dawid Kutyła [1] and Piotr Żabiński [1]

[1] Faculty of Non-Ferrous-Metals, AGH University of Krakow, al. Adama Mickiewicza, 30-059 Krakow, Poland
[2] Chemistry Department, Faculty of Science, Tanta University, Tanta 31527, Egypt
* Correspondence: kskib@agh.edu.pl

Abstract: Ni–Cu alloys are suitable candidates as catalysts in hydrogen evolution reaction. Because of the different magnetic properties of Ni and Cu, the influence of an applied external magnetic field on the synthesis Ni–Cu alloys was studied. The coatings were prepared with visible changes in their appearance. The differences between the observed regions were studied in terms of morphology and chemical composition. In addition, the overall chemical and phase compositions were determined using X-ray fluorescence and X-ray diffraction methods, respectively. The catalytic activity was measured in 1 M NaOH using linear sweep voltammetry. The contact angle was determined using contour analysis. All samples were hydrophilic. Hydrogen evolution started at different times depending on the area on the surface. It started earliest on the coating obtained in parallel to the electrode magnetic field at 250 mT. We found that when the Lorenz force is maximal, Cu deposition is preferred because of the enhancement of mass transport.

Keywords: Ni–Cu alloys; magnetic field; Lorentz force; hydrogen evolution

Citation: Skibińska, K.; Elsharkawy, S.; Kołczyk-Siedlecka, K.; Kutyła, D.; Żabiński, P. Influence of the Applied External Magnetic Field on the Deposition of Ni–Cu Alloys. *Metals* **2024**, *14*, 281. https://doi.org/10.3390/met14030281

Academic Editor: Nebojša Nikolić

Received: 5 February 2024
Revised: 17 February 2024
Accepted: 25 February 2024
Published: 28 February 2024

1. Introduction

The deposition of Ni–Cu alloys has been well studied in the literature [1–3]. They exhibit high microhardness and good corrosion resistance [4]. When the current density increases, the Ni content is higher [5,6]. The morphology of the coating is related to the kinetic control and efficiency of the electroplating process [7]. The alloys crystallize in a face-centered cubic structure [8], and at a higher pH, the larger crystallites of the alloy are grown [9]. In addition, as the pH increases, the Cu content also increases [9]. The lamellar Ni/Cu multilayers can be electrochemically synthesized [10].

Magnetoelectrodeposition involves the application of magnetic fields during the electrodeposition process, which can influence the microstructure, morphology, and properties of the deposited layers. The research in this area explores various aspects of how magnetic fields affect the deposition process and the resulting films. The most important factors that need to be taken into consideration are the hydrodynamics of the electrolyte influenced by the magnetic field. This additional force affects the transport of ions to the electrode surface. Magnetohydrodynamic (MHD) convection can enhance mass transfer, leading to more uniform deposition but may also introduce vortices that affect the deposition pattern. Moreover, the intensity and direction of the applied magnetic field are crucial. They directly influence the magnetohydrodynamic (MHD) effects that alter the mass transfer and the deposition kinetics at the electrode surface. The magnetic field can enhance or disturb the deposition process, affecting the morphology, grain size, and orientation of the deposited film. Last but not least is the magnetic susceptibility of ions present in the electrolyte.

Ni and Cu are two elements that are characterized by different magnetic properties, so we expect the magnetohydrodynamic (MHD) effect to have a strong influence during electrodeposition. The presence of the magnetic field improved the corrosion resistance

and microhardness of Ni coatings [11]. The synthesized layers are also fine-grained [12]. The magnetic field can also be used for electroless deposition of Ni and its alloys [13,14].

The influence of a low-intensity magnetic field (0.5 to 0.7 mT) on the deposition of Cu was also observed [15]. Changes in, inter alia, the texture and morphology of the Cu surface appeared. The creation of the MHD effect, especially with the application of medium-intensity magnetic fields (0.6 T), can be used to tailor the chemical composition of nanostructures based on anodic alumina membranes, in terms of Co, Co–Fe, and Co–Ru systems [16,17]. The impact of the MHD phenomenon is usually considered in numerical simulations using OpenFOAM [18] or Comsol V 5.6 software [19,20]. The outcome is compared with the experimental results. The MHD effect is usually applied in microfluidic systems [21]. Moreover, a lot of attention is paid to magneto-electrochemistry as a field of study focused on, inter alia, enhancing the electrocatalytic performance with the magnetic field [22,23]. When the magnetic field is applied, the value of the Tafel slope is lower [24]. The water and hydroxide ions are characterized by different diamagnetic properties; therefore, the concentration gradient of hydroxide ions near the electrode surface is affected by the external magnetic field [25]. Additionally, the MHD phenomenon can be used to create localized micro-MHD vortices and can therefore enhance the kinetics of the reaction [26].

Nickel and its alloys are esteemed for their superior electrocatalytic abilities, notably in promoting the hydrogen evolution reaction (HER), rendering them essential for a wide range of electrochemical operations. Specifically, nickel and its diverse alloys are the preferred choice for electrode materials in alkaline water electrolysis due to their remarkable performance. The efficiency of nickel in the HER can be greatly improved through the formation of alloys with specific elements, which induces a synergistic effect well documented in scientific research [27,28]. While the development of nickel alloys with noble metals such as palladium [29–31], platinum [32–34], ruthenium [35–38], and rhodium [39–43] presents a promising avenue for new material innovations, the high costs associated with these noble metals and the necessary precursors for their electrodeposition processes have shifted focus towards more economically viable nickel-based alloys with transition metals like cobalt [44–46], tungsten/molybdenum [47–50], and copper. These alloys are generally fabricated via electrodeposition, where incorporating transition metals changes the reaction mechanism of the electrodes, thus affecting the activation energy required for the HER. The choice of alloying metals and electrodeposition conditions critically influences the physical and chemical properties of the resulting nickel-based alloy electrodes, impacting their electrocatalytic effectiveness for the HER. Among these, the Ni–Cu alloy stands out as an especially promising candidate for cathodes in alkaline HER on the basis of its outstanding electrocatalytic activity, excellent corrosion resistance, high abundance, and affordability.

Tri-component alloys like Ni–Co–Cu and Ni–Mo–Cu, electrodeposited under various conditions by D. Goranova et al. [51], have shown significant electrocatalytic activity for HER in alkaline media. The incorporation of copper improves the catalytic activity, with Ni43Co37Cu20 and Ni57Mo27Cu16 alloys displaying the best performance due to a combination of surface area development and Ni–Co synergism. Negem et al. [52] electrodeposited Ni–Cu nanocrystalline alloys based on glycine-type electrolytes, and they reported that these alloys were more active than pure nickel for hydrogen evolution reactions in alkaline solutions. The optimization of Ni–Cu compositions based on different nickel–copper ratios and the creation of nanocrystalline structures were key to enhancing HER activity. Chemical and phase composition can be useful for tailoring the catalytic activity due to the synergetic effect between elements, but the morphology and surface development also play a crucial role in modifying the overpotential in the hydrogen evolution reaction. This effect was reported by Cui et al. [53], who showed that porous Ni–Cu alloy films composed of nanosheets, created via potentiostatic electrodeposition, exhibited enhanced electrocatalytic activity for HER in alkaline media. This enhancement was attributed to the formation of nanoporous structures with a large number of active sites. These studies collectively highlight the potential of Ni–Cu alloys, obtained through electrodeposition, as effective catalysts for hydrogen evolution in alkaline environments.

The specific composition and structural characteristics of these alloys play crucial roles in their catalytic performance.

Based on previously mentioned works, there are no doubts that Ni–Cu alloys can be successfully obtained using the electrodeposition method. However, no studies have been conducted to investigate the influence of the applied magnetic field on the co-deposition of these metals. This is of interest because of the different magnetic properties of Ni and Cu. In this work, the magnetic field was applied in two different directions at two intensities (250 and 500 mT). The obtained coatings were carefully analyzed via many methods. The influence of the MHD effect is also discussed.

2. Materials and Methods

Ni–Cu coatings were deposited from the electrolyte containing 0.2 M $C_6H_5Na_3O_7 \cdot 2H_2O$, 0.1 M $CuSO_4 \cdot 5H_2O$, and 0.8 M $NiSO_4 \cdot 6H_2O$ at 10 mA/cm^2 for 10 min. The pH was adjusted to 9 with 25% NH_3 solution. The substrate Cu foil with the deposited layer of metallic Co (Cu/Co) was used to avoid the signals overlapping from the substrate and the deposited layer during the chemical analysis. The conventional three-electrode cell was used with Cu/Co as the working electrode, Pt mesh as the counter electrode, and saturated calomel electrode (SCE) (Eurosensor, Giwice, Poland) as the reference electrode. The electrodeposition was performed with a SP200 BioLogic potentiostat (Bio-Logic Science Instruments SAS, Seyssinet-Pariset, France).

The magnetic field (250 and 500 mT) was applied using an electromagnet LakeShore EM4-HVA (Lake Shore Cryotronics, Inc., Westerville, OH, USA) equipped with power supplier LakeShore Model 642 (Lake Shore Cryotronics, Inc., Westerville, OH, USA). The top view of the schematics of the setup is shown in Figure 1.

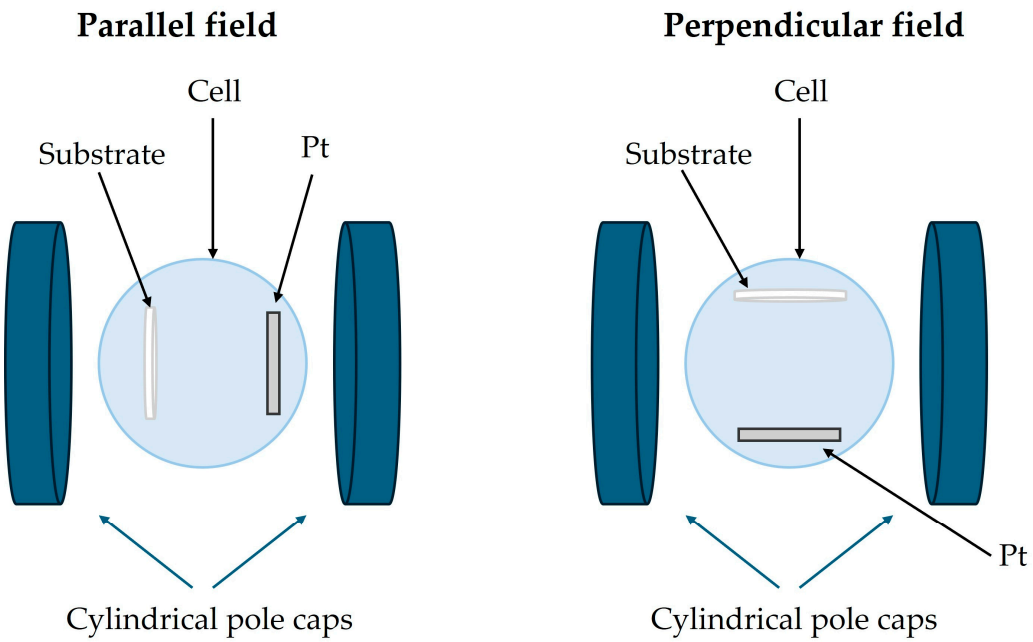

Figure 1. Schemes of the experimental setups (top views).

The parallel direction of the magnetic field corresponds to the relation between lines of magnetic and electric fields, as shown in Figure 1. The sample was placed in the center where the lines of the magnetic field were parallel to each other. Additionally, the sample's diameter was about 5 times smaller than the diameter of the magnets' cylindrical pole caps. By applying these procedures, the homogeneity of the magnetic field was ensured.

A detailed analysis of the coatings was carried out using a JEOL-6000 Plus scanning electron microscope (SEM) (JEOL, Tokyo, Japan) equipped with an energy dispersive X-ray spectrometer (EDS). The chemical composition was also determined using X-ray fluores-

cence (XRF) with a Rigaku Primini (Tokyo, Japan). X-ray diffraction (XRD) measurements were performed with a Rigaku MiniFlex II apparatus (Tokyo, Japan) equipped with a Cu lamp.

The values of the contact angles were determined through contour analysis utilizing Image J V 1.8.0 software. A 10 µL droplet of deionized water was applied to the surface of each sample three times. The measurements were performed using a high-speed camera Model:9501 with HiBestViewer 1.0.5.1 software.

The catalytic properties were determined in 1 M NaOH using the SP200 BioLogic potentiostat. The geometric surface area (2.8 cm^2) was assumed to be the active surface area. Ni–Cu alloys were used as the working electrode, Pt mesh as the counter electrode, and SCE as the reference electrode. Linear sweep voltammetry (LSV) was performed at a scan rate of 20 mV/s from the open-circuit potential (OCP) value to −1.6 V vs. SCE. The ohmic drop determination technique was used prior to each LSV measurement, and the Tafel slopes were determined using the LSV curves.

3. Results

The coatings were deposited as described above. A detailed characterization of their composition and morphology as well as their properties was performed.

3.1. Morphology and Composition

The influence of the applied external magnetic field on the obtained coatings was visible in the appearance of the samples (Figure 2). At both intensities in the parallel magnetic field, the color associated with the presence of Cu could be distinguished. The same phenomenon appeared on the surface of the sample deposited at 500 mT in the perpendicular magnetic field. The central area was chosen to analyze the sample obtained without the applied magnetic field. In the case of the coatings deposited in the present magnetic field, the characteristic areas of analysis were selected. They are shown in Figure 3.

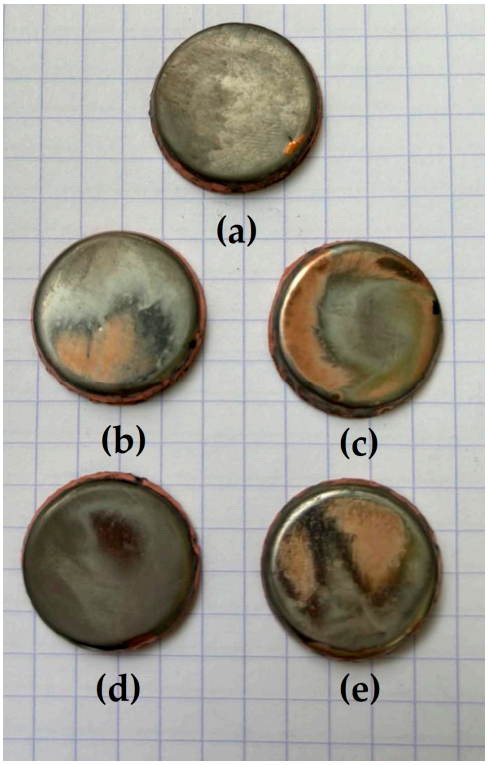

Figure 2. Photos of the coatings obtained (**a**) without and with (**b**,**c**) parallel and (**d**,**e**) perpendicular magnetic fields at 250 (**b**,**d**) and 500 mT (**c**,**e**).

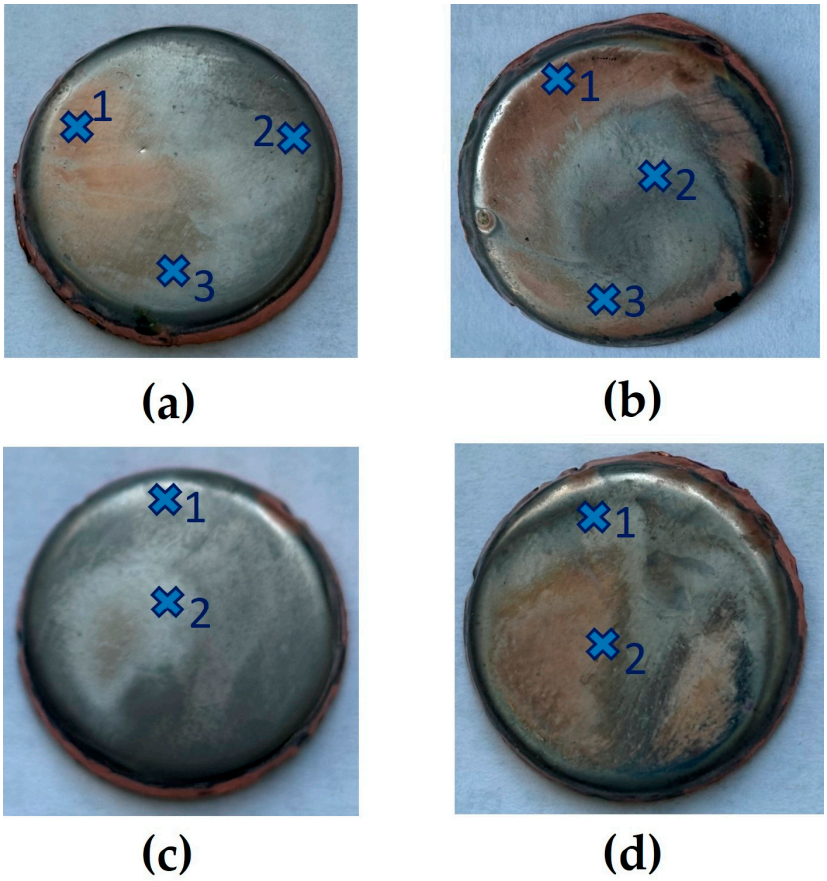

Figure 3. Photos with the marked places of SEM/EDS analysis: (**a**,**b**) parallel and (**c**,**d**) perpendicular magnetic fields at (**a**,**c**) 250 and (**b**,**d**) 500 mT.

The main areas were chosen on the basis of the color (orange/silver) or the degree of shine (metallic or shineless). The SEM photos are shown in Figure 4, and the magnification is ×2000.

The areas on the same sample that were deposited in the applied magnetic field are characterized by different morphologies. For all samples, light grey, slightly shiny surfaces show similar microstructures (Figure 4(a,b-2,b-3,c-2,d-1,e-1). However, the morphology in the copperish color varies between the samples (Figure 4(b-1,c-1,e-2)). These changes may relate to the local chemical compositions. To confirm this, EDS analyses were performed, and the results are listed in Table 1.

Table 1. Chemical composition analyzed using the EDS method.

Sample	Point	Chemical Composition, [% at.]		
		Cu	Ni	O
0 mT	-	47.7	49.6	2.7
250 mT parallel	1	80.1	16.7	3.2
	2	35.5	61.3	3.2
	3	62.7	35.1	2.2
500 mT parallel	1	82.2	3.6	14.2
	2	34.1	61.3	4.6
	3	29.0	65.8	5.2
250 mT perpendicular	1	50.1	46.8	3.1
	2	66.1	31.8	2.1
500 mT perpendicular	1	36.1	59.9	4.0
	2	77.0	8.2	14.8

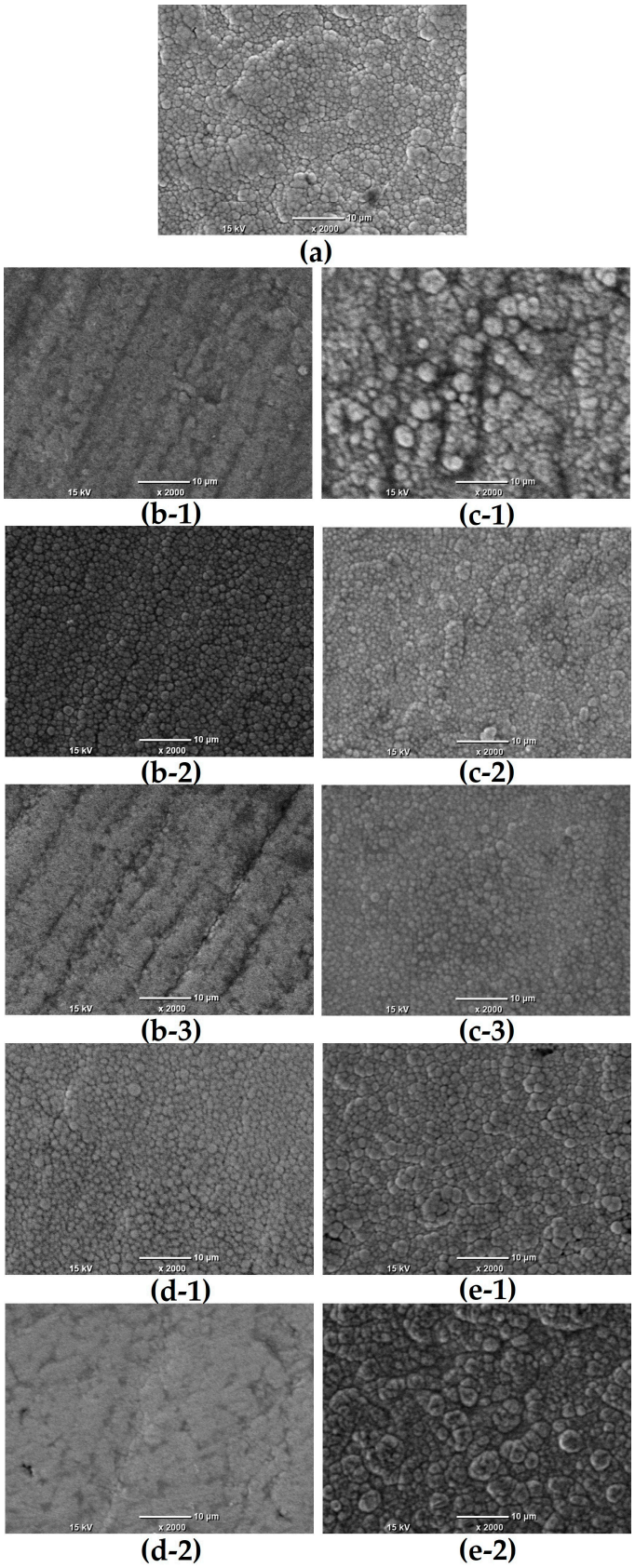

Figure 4. SEM photos of coatings obtained (**a**) without and with (**b-1**–**c-3**) parallel and (**d-1**–**e-2**) perpendicular magnetic fields at 250 (**b-1**–**b-3**,**d-1**,**d-2**) and 500 mT (**c-1**–**c-3**,**e-1**,**e-2**). Numbers 1–3 correspond to the areas on the sample marked in Figure 3. Letters a-e correspond to Figure 2.

The sample deposited without the applied magnetic field was composed of both Cu and Ni in similar amounts. All the areas with the copperish color were characterized by a high content of Cu (77–82 at. %) and a low content of Ni (3–16 at. %). At 500 mT, for both directions of the magnetic field, there was about 15 at. % of oxygen. Other similar regions were Ni–Cu alloys with a Cu content between 30 and 50 at. %. If the Cu content was more than 50 but less than 77 at. %, the area had a bright silver-copperish color.

The overall chemical composition was investigated using the XRF method. This technique allows the determination of elemental composition using the interaction of X-rays with a material. The results are listed in Table 2.

Table 2. Chemical composition determined using the XRF method.

Sample	Chemical Composition [% Mass]	
	Cu	Ni
0 mT	54.15	45.85
250 mT parallel	70.69	29.31
500 mT parallel	77.38	22.62
250 mT perpendicular	54.75	45.25
500 mT perpendicular	76.69	23.31

At both intensities, the application of the parallel magnetic field increased the Cu content in the coatings. In the case of the perpendicular direction, the amount of copper did not change at 250 mT, but it was higher at 500 mT.

The possible influence of the magnetic field on the phase composition of the alloys was investigated using the XRD method. The obtained patterns are shown in Figure 5.

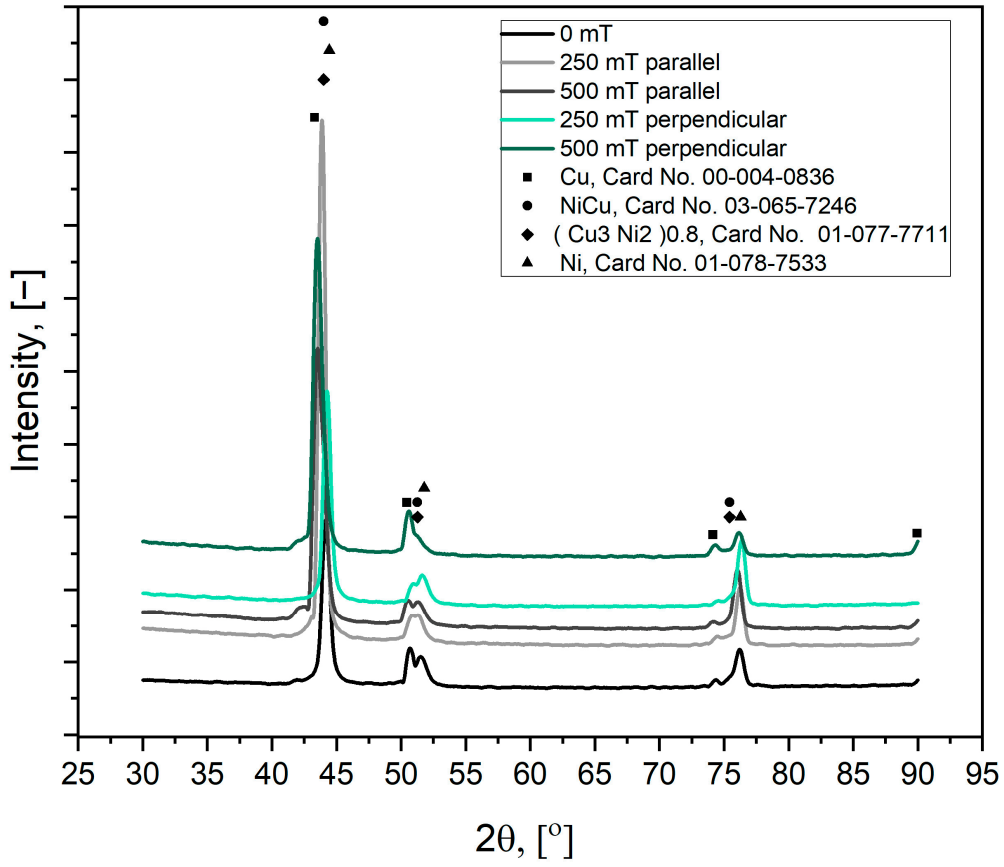

Figure 5. X-ray diffraction patterns.

The impact of the magnetic fields on the phase composition of the electrodeposited films was notably significant, as evidenced by peaks within a specific range of angles, particularly from 50 to 53 degrees. These modifications in phase composition are indicative of the magnetic field's role in influencing the structural properties of the deposited films. For instance, in the sample prepared without the application of a magnetic field (0 mT), two distinct peaks were discernible. These peaks, representative of certain phase compositions, were consistently observed across various samples. However, an exception was noted for the sample deposited at a magnetic field strength of 500 mT oriented perpendicularly to the deposition surface. In this case, the peak corresponding to pure copper (Cu) exhibited a significantly heightened intensity compared to those associated with nickel (Ni), nickel–copper (Ni–Cu), and copper–nickel (Cu–Ni) phases.

Furthermore, the intensity of the peak at 76°, which was attributed to the Ni, Ni–Cu, or Cu–Ni phases, underwent a noticeable increase under the influence of magnetic fields applied both parallelly (at strengths of 250 and 500 mT) and perpendicularly (at 250 mT). This suggests that the application of magnetic fields, regardless of their orientation, can enhance the presence or crystallinity of these phases. Interestingly, at a magnetic field strength of 500 mT applied in a perpendicular orientation, the intensity of this particular peak was found to be lower than that observed in the absence of a magnetic field (0 mT). Concurrently, the peak denoting the presence of Cu became more pronounced, indicating a preferential growth or enrichment of the copper phase under these conditions.

The crystallite size was determined using the Scherrer equation. The X-ray wavelength was 0.15418 nm (Copper K-α), and the chosen peak was ~76°. For each sample, the full width at a half maximal peak height was measured on the basis of Figure 5, and the results are shown in Table 3.

Table 3. Results of crystallite size based on the Scherrer equation.

Sample	Crystallite Size [nm]
0 mT	12
250 mT parallel	13
500 mT parallel	13
250 mT perpendicular	12
500 mT perpendicular	15

We assumed that the crystallite size was related to the Ni–Cu alloy. There was no strong influence of the applied magnetic field. However, a change was visible for the coating deposited at 500 mT in the perpendicular magnetic field: the crystallites of this sample were the largest. The influence of the parallel magnetic field can be omitted.

The observed variations in peak intensities and phase compositions under different magnetic field strengths and orientations highlight the magnetic field's capacity to alter the microstructural characteristics of the films. This phenomenon can be attributed to the magnetohydrodynamic effects induced by the magnetic field, which influence the ion transportation and deposition dynamics during the electrodeposition process. By affecting the deposition kinetics and the ion flux towards the substrate, magnetic fields can thus play a pivotal role in dictating the phase composition, crystallinity, and overall catalytic properties of the deposited films.

3.2. Catalytic Activity

The catalytic activity was analyzed on the basis of wettability and LSV measurements.

The wettability of the coatings was measured through contour analysis. Each measurement was repeated three times. The average value was calculated, and the results are listed in Table 4.

Table 4. Results of the wettability measurements.

Sample	Contact Angle [°]
0 mT	71 ± 4
250 mT parallel	73 ± 8
500 mT parallel	71 ± 8
250 mT perpendicular	68 ± 7
500 mT perpendicular	65 ± 7

All coatings were hydrophilic. The samples deposited in the perpendicular magnetic field showed slightly lower contact angles.

The LSV measurements are shown in Figure 6.

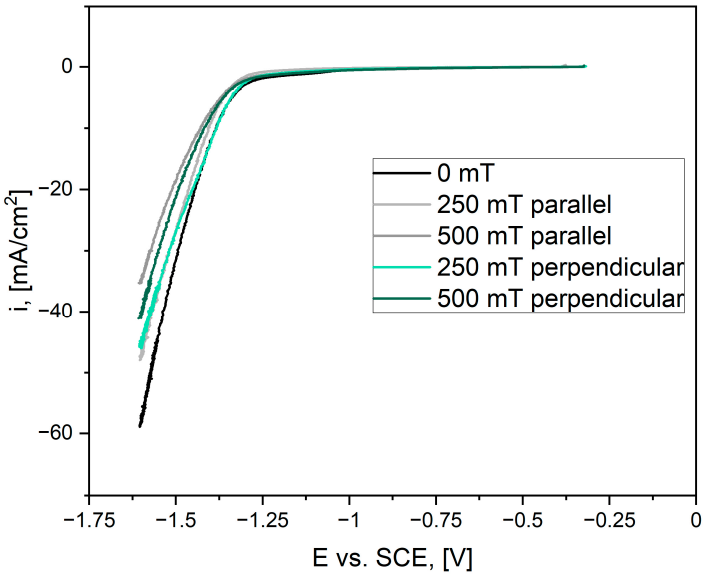

Figure 6. LSV curves obtained for all coatings. Curves with 85% IR-drop compensation.

The application of the magnetic field did not increase the catalytic activity of the coatings. The best performance, in terms of current density and slope of the curve, was observed for the sample deposited at 0 mT. Conversely, the coating deposited at 500 mT in the parallel magnetic field had the worst catalytic properties. Moreover, for both directions, the stronger the magnetic field, the worse the activity. Using the LSV curves, the potential E_{ONSET} at which the hydrogen evolution started was determined in the following way: two tangents were plotted on the curve of the potential dependence on the current density, and the point of their intersection indicated the ONSET potential. Its values are given in Table 5.

Table 5. Values of E_{ONSET}.

Sample	E_{ONSET} [V]
0 mT	−1.38
250 mT parallel	−1.35
500 mT parallel	−1.37
250 mT perpendicular	−1.33
500 mT perpendicular	−1.38

The evolution of the hydrogen started the earliest on the sample deposited at 250 mT in the perpendicular magnetic field. For the rest of the samples, the potential varied slightly. The values of the Tafel slope were determined on the basis of the curves in Figure 6, and the results are listed in Table 6.

Table 6. Results of the Tafel slope determination.

Sample	Tafel Slope [mV/dec]
0 mT	172
250 mT parallel	143
500 mT parallel	181
250 mT perpendicular	138
500 mT perpendicular	173

The application of the magnetic field with the lower intensity decreased the value of the Tafel slope compared with the sample deposited without the magnetic field.

Additionally, hydrogen bubbles were observed during their evolution. The photos are shown in Figure 7. The characteristic points are marked in the photos to show how the sample is set in the Teflon holder.

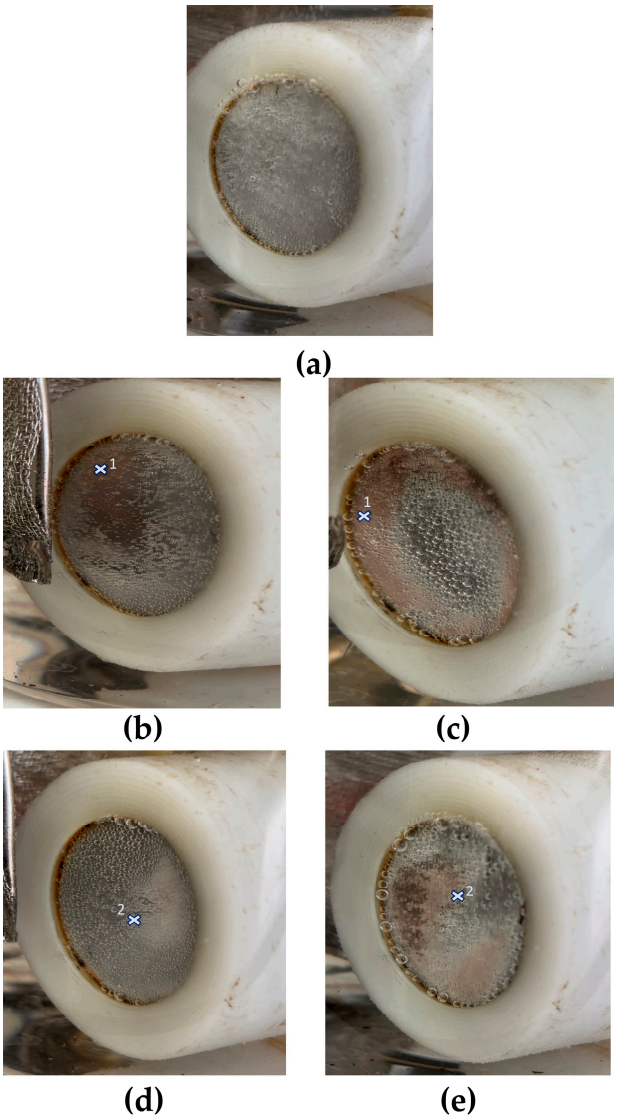

Figure 7. Photos of the hydrogen bubbles at the beginning of the hydrogen evolution on the samples deposited (**a**) without and with (**b**,**c**) parallel and (**d**,**e**) perpendicular magnetic fields at 250 (**b**,**d**) and 500 mT (**c**,**e**).

The evolution of hydrogen took place over the whole area of the sample deposited at 0 mT (Figure 7a). However, for the other samples, there were differences between the areas

of the sample. We observed that the process started later for all the copper areas compared to the silver areas.

The time after which the hydrogen HER started is listed in Table 7. The time corresponds to E_{ONSET} as the approximate value for each sample. Reading the time from the videos and photographs is not suitable because the bubbles were the result of the coalescence of many little bubbles that were invisible at the beginning.

Table 7. Time after which the HER started.

Sample	Time [s]
0 mT	192
250 mT parallel	188
500 mT parallel	192
250 mT perpendicular	190
500 mT perpendicular	192

Since the scans started from the OCP value, the time needed to obtain E_{ONSET} differed for each sample. The fastest evolution was initiated for the sample deposited at 250 mT in the parallel magnetic field. However, the differences between the coatings were slight.

4. Discussion

Ni–Cu alloy coatings were successfully deposited under the applied conditions. The magnetic field with two directions (parallel and perpendicular) was applied during the synthesis of the samples. Its influence was strongly visible in the appearance of the sample surface in both directions and at both intensities. When the magnetic field is perpendicular (parallel to the electrode), the Lorentz force reaches the maximum [54]. On the surface it was visible as separated regions. In the parallel magnetic field there were eddies, especially at 500 mT, probably caused by global flow, which also affects the mass transport. The global flow was observed in a similar setup used for the deposition of Ni cones [55]. These varieties are related to the differences in the chemical composition. The morphology of the brighter and darker silverish regions corresponded to Ni–Cu alloys, and our results are in accordance with the literature [5]. The general chemical composition analyzed with the XRF method allowed us to conclude that when the Lorentz force is minimal, the Cu content increases. At the same time, when the magnetic field was parallel-to-electrode, the amount of copper did not change at 250 mT, but it was higher at 500 mT. However, this phenomenon is strictly connected with the surface of copperish areas. The larger they are, the more Cu is detected. Moreover, the applied magnetic field also affected the phase composition of the coatings. The peaks could not be easily distinguished because of their similar positions. However, the intensity of Ni, Ni–Cu, or Cu–Ni peaks at 76° increased when the perpendicular-to-electrode (at 250 and 500 mT) and parallel-to-electrode magnetic fields (at 250 mT) were applied. As there are no studies on the electrodeposition of Ni–Cu in a magnetic field, it is believed that the strong MHD effect present at 500 mT promotes the deposition of Cu. Literature reviews show that Cu is reduced under the control of mass transport [56,57]. Therefore, the enhancement of this phenomenon by the MHD effect caused the increase in Cu content at 500 mT in the perpendicular (parallel to the electrode) magnetic field. When the intensity was lower, there was no effect on the overall chemical composition. However, it appeared and was clearly visible in the appearance of the coating. The absence of the magnetic field allowed the Ni–Cu alloys to be deposited homogeneously over the entire substrate. The content of Ni sulfate in the electrolyte was much higher than the Cu sulfate content. However, because of the preferential reduction of Cu^{2+} ions over Ni^{2+} ions, the amounts of both elements were similar for the coating [58,59].

In the case of the catalytic properties, the perpendicular (parallel to the electrode) magnetic field slightly decreased the wettability of the coatings. This may be related to the probable lower roughness of the coatings caused by the MHD effect. All samples were hydrophilic, which means that the hydrogen bubbles should become smaller and

leave the surface faster [60]. Ni coatings deposited in the magnetic field had hydrophobic properties [61]. In the case of the Ni–Cu alloy, the contact angle values were lower. However, the magnetic field decreased the catalytic activity based on the slopes and values of the current densities even though the evolution of hydrogen started earliest on the sample deposited at 250 mT in the perpendicular magnetic field. This sample also had the lowest Tafel slope value. In the literature, this value is about 140 mV/dec for Ni–Cu alloys [62]. The chemical composition of this coating was similar to that of the coating obtained at 0 mT. However, there were slight differences in the phase composition. Please note that the catalytic results were approximate for the different surfaces of each sample. In addition, the hydrogen evolution of these surfaces was observed. The process started later on the coppery surfaces than on the silvery ones. This is due to the better catalytic activity of Ni than Cu. For the sample synthesized without the magnetic field, the whole surface was equally active. This phenomenon concludes the consequences of the differences in phase composition.

5. Conclusions

Ni–Cu alloys are suitable candidates as catalysts in HER. The influence of the applied magnetic field in two directions at two intensities was analyzed using many different methods. We conclude that the present magnetic field strongly affected the appearance of the obtained alloys. Consequently, it caused alterations in the chemical compositions and morphologies of the samples' surfaces. The impacts of the varying areas are evident because the hydrogen evolution started at different times. However, our results regarding the wettability and LSV measurements deliver the approximate values for the whole surface. Therefore, the best catalytic activity was shown with the coating obtained without the applied magnetic field, even if this evolution was initiated the earliest on the surface produced in the perpendicular magnetic field at 250 mT. Our results highlight the importance of the local surface characteristics on the overall properties of the coating. Because of the various applications of Ni–Cu alloys, e.g., superhydrophobic coatings [63], supercapacitors [64], or methanol electrooxidation [65], these results could yield some important observations for other groups.

Author Contributions: Conceptualization, K.S.; formal analysis, K.S.; investigation, K.S., S.E., K.K.-S. and D.K.; writing—original draft preparation, K.S. and S.E.; writing—review and editing, D.K., K.K.-S. and P.Ż.; supervision, P.Ż.; funding acquisition, K.S. All authors have read and agreed to the published version of the manuscript.

Funding: This research was funded by the Polish National Science Centre (NCN), with grant number UMO-2022/45/N/ST5/00226.

Data Availability Statement: The original contributions presented in the study are included in the article, further inquiries can be directed to the corresponding author.

Conflicts of Interest: The authors declare no conflicts of interest.

References

1. Sarac, U.; Öksüzoğlu, R.M.; Baykul, M.C. Deposition potential dependence of composition, microstructure, and surface morphology of electrodeposited Ni–Cu alloy films. *J. Mater. Sci. Mater. Electron.* **2012**, *23*, 2110–2116. [CrossRef]
2. Chassaing, E.; Quang, K.V.; Wiart, R. Mechanism of copper-nickel alloy electrodeposition. *J. Appl. Electrochem.* **1987**, *17*, 1267–1280. [CrossRef]
3. Wang, S.; Guo, X.; Yang, H.; Dai, J.; Zhu, R.; Gong, J.; Peng, L.; Ding, W. Electrodeposition mechanism and characterization of Ni–Cu alloy coatings from a eutectic-based ionic liquid. *Appl. Surf. Sci.* **2014**, *288*, 530–536. [CrossRef]
4. Staroń, S.; Ledwig, P.; Dubiel, B. Electrodeposited Ni-Cu Coatings with Hierarchical Surface Morphology. *Metall. Mater. Trans. A* **2022**, *53*, 2071–2085. [CrossRef]
5. Goranova, D.; Avdeev, G.; Rashkov, R. Electrodeposition and characterization of Ni-Cu alloys. *Surf. Coat. Technol.* **2014**, *240*, 204–210. [CrossRef]
6. Ngamlerdpokin, K.; Tantavichet, N. Electrodeposition of nickel-copper alloys to use as a cathode for hydrogen evolution in an alkaline media. *Int. J. Hydrog. Energy* **2014**, *39*, 2505–2515. [CrossRef]

7. Brito, M.M.; Artisiani, R.A.; Carlos, I.A. The electrodeposition of Ni-Cu and Ni-Cu-P from aspartate-based baths. *J. Alloys Compd.* **2022**, *890*, 161761. [CrossRef]
8. Kockar, H.; Bayirli, M.; Alper, M. A new example of the diffusion-limited aggregation: Ni–Cu film patterns. *Appl. Surf. Sci.* **2010**, *256*, 2995–2999. [CrossRef]
9. Alper, M.; Baykul, M.C.; Péter, L.; Tóth, J.; Bakonyi, İ. Preparation and Characterisation of Electrodeposited Ni–Cu/Cu Multilayers. *J. Appl. Electrochem.* **2004**, *34*, 841–848. [CrossRef]
10. Myung, N.V.; Nobe, K. Electrodeposition of Ni/Cu multilayers. *Trade J.* **2000**, *87*, 125–134.
11. Basori; Soegijono, B.; Susetyo, F.B. Magnetic field exposure on electroplating process of ferromagnetic nickel ion on copper substrate. *J. Phys. Conf. Ser.* **2022**, *2377*, 012002. [CrossRef]
12. Bund, A.; Ispas, A.; Mutschke, G. Magnetic field effects on electrochemical metal depositions. *Sci. Technol. Adv. Mater.* **2008**, *9*, 024208. [CrossRef]
13. Kołczyk-Siedlecka, K.; Kutyła, D.; Skibińska, K.; Jędraczka, A.; Żabiński, P. Catalytic Properties of Electroless Nickel-Based Coatings Modified by the Magnetic Field. *Arch. Met. Mater* **2024**, *69*, 17–24.
14. Kołczyk-Siedlecka, K.; Skibińska, K.; Kutyła, D.; Kwiecińska, A.; Kowalik, R.; Żabiński, P. Influence of magnetic field on electroless metallization of 3D prints by copper and nickel. *Arch. Metall. Mater.* **2019**, *64*, 17–22. [CrossRef]
15. Kovalyov, S.V.; Girin, O.B.; Debiemme-Chouvy, C.; Mishchenko, V.I. Copper electrodeposition under a weak magnetic field: Effect on the texturing and properties of the deposits. *J. Appl. Electrochem.* **2021**, *51*, 235–243. [CrossRef]
16. Dobosz, I.; Kutyła, D.; Kac, M.; Włoch, G.; Żabiński, P. The influence of homogenous external magnetic field on morphology and magnetic properties of CoRu nanowire arrays. *Mater. Sci. Eng. B Solid-State Mater. Adv. Technol.* **2020**, *262*, 114795. [CrossRef]
17. Hang, T.; Hu, A.; Li, M.; Mao, D. Structural control of a cobalt nanocone array grown by directional electrodeposition. *CrystEngComm* **2010**, *12*, 2799–2802. [CrossRef]
18. Huang, M.; Weber, N.; Mutschke, G. A Simulation Framework for Electrochemical Processes with Electrolyte Flow. *J. Electrochem. Soc.* **2023**, *170*, 073502. [CrossRef]
19. Huang, M.; Uhlemann, M.; Eckert, K.; Mutschke, G. Pulse Reverse Plating of Copper Micro-Structures in Magnetic Gradient Fields. *Magnetochemistry* **2022**, *8*, 66. [CrossRef]
20. Liang, P.; Li, Q.; Chen, L.; Tang, Z.; Li, Z.; Wang, Y.; Tang, Y.; Han, C.; Lan, Z.; Zhi, C.; et al. The magnetohydrodynamic effect enables a dendrite-free Zn anode in alkaline electrolytes. *J. Mater. Chem. A* **2022**, *10*, 11971–11979. [CrossRef]
21. Bau, H.H. Applications of Magneto Electrochemistry and Magnetohydrodynamics in Microfluidics. *Magnetochemistry* **2022**, *8*, 140. [CrossRef]
22. Mitra, K.; Adalder, A.; Mandal, S.; Ghorai, U.K. Enhancing Electrochemical Reactivity with Magnetic Fields: Unraveling the Role of Magneto-Electrochemistry. *Small Methods* **2024**, e2301132. [CrossRef]
23. Luo, S.; Elouarzaki, K.; Xu, Z.J. Electrochemistry in Magnetic Fields. *Angew. Chemie Int. Ed.* **2022**, *61*, e202203564. [CrossRef]
24. Zhou, W.; Chen, M.; Guo, M.; Hong, A.; Yu, T.; Luo, X.; Yuan, C.; Lei, W.; Wang, S. Magnetic Enhancement for Hydrogen Evolution Reaction on Ferromagnetic MoS 2 Catalyst. *Nano Lett.* **2020**, *20*, 2923–2930. [CrossRef]
25. Sambalova, O.; Billeter, E.; Yildirim, O.; Sterzi, A.; Bleiner, D.; Borgschulte, A. Magnetic field enhancement of electrochemical hydrogen evolution reaction probed by magneto-optics. *Int. J. Hydrogen Energy* **2021**, *46*, 3346–3353. [CrossRef]
26. Salinas, G.; Lozon, C.; Kuhn, A. Unconventional applications of the magnetohydrodynamic effect in electrochemical systems. *Curr. Opin. Electrochem.* **2023**, *38*, 101220. [CrossRef]
27. Deng, Y.; Lai, W.; Xu, B. A Mini Review on Doped Nickel-Based Electrocatalysts for Hydrogen Evolution Reaction. *Energies* **2020**, *13*, 4651. [CrossRef]
28. Angeles-Olvera, Z.; Crespo-Yapur, A.; Rodríguez, O.; Cholula-Díaz, J.; Martínez, L.; Videa, M. Nickel-Based Electrocatalysts for Water Electrolysis. *Energies* **2022**, *15*, 1609. [CrossRef]
29. Zhao, M.; Wu, Y.; Cai, W.; Xia, T.; Jiang, W.-J.; Ding, W.; Cao, J.-P. Boosting hydrogen evolution activity and durability of Pd–Ni–P nanocatalyst via crystalline degree and surface chemical state modulations. *Int. J. Hydrogen Energy* **2019**, *44*, 31053–31061. [CrossRef]
30. Mech, K.; Wróbel, M.; Wojnicki, M.; Mech-Piskorz, J.; Żabiński, P.; Kowalik, R. Electrodeposition of NiPd alloy from aqueous chloride electrolytes. *Appl. Surf. Sci.* **2016**, *388*, 809–816. [CrossRef]
31. Tang, J.; Zhao, X.; Zuo, Y.; Ju, P.; Tang, Y. Electrodeposited Pd-Ni-Mo film as a cathode material for hydrogen evolution reaction. *Electrochim. Acta* **2015**, *174*, 1041–1049. [CrossRef]
32. Fukumoto, M.; Takahashi, H.; Kutyła, D.; Wojnicki, M.; Żabiński, P. Morphological investigation and electrochemical performance evaluation of novel porous Ni–Pt produced by Al-deposition/dissolution in molten salts for hydrogen and oxygen evolution reaction. *Int. J. Hydrogen Energy* **2023**, *49*, 754–765. [CrossRef]
33. Fiameni, S.; Herraiz-Cardona, I.; Musiani, M.; Pérez-Herranz, V.; Vázquez-Gómez, L.; Verlato, E. The HER in alkaline media on Pt-modified three-dimensional Ni cathodes. *Int. J. Hydrogen Energy* **2012**, *37*, 10507–10516. [CrossRef]
34. Eiler, K.; Krawiec, H.; Kozina, I.; Sort, J.; Pellicer, E. Electrochemical characterisation of multifunctional electrocatalytic mesoporous Ni-Pt thin films in alkaline and acidic media. *Electrochim. Acta* **2020**, *359*, 136952. [CrossRef]
35. Kutyła, D.; Kołczyk-Siedlecka, K.; Kwiecińska, A.; Skibińska, K.; Kowalik, R.; Żabiński, P. Preparation and characterization of electrodeposited Ni-Ru alloys: Morphological and catalytic study. *J. Solid State Electrochem.* **2019**, *23*, 3089–3097. [CrossRef]

36. Liu, J.; Wang, J.; Fo, Y.; Zhang, B.; Molochas, C.; Gao, J.; Li, W.; Cui, X.; Zhou, X.; Jiang, L.; et al. Engineering of unique Ni-Ru nano-twins for highly active and robust bifunctional hydrogen oxidation and hydrogen evolution electrocatalysis. *Chem. Eng. J.* **2023**, *454*, 139959. [CrossRef]
37. Mao, J.; He, C.-T.; Pei, J.; Liu, Y.; Li, J.; Chen, W.; He, D.; Wang, D.; Li, Y. Isolated Ni Atoms Dispersed on Ru Nanosheets: High-Performance Electrocatalysts toward Hydrogen Oxidation Reaction. *Nano Lett.* **2020**, *20*, 3442–3448. [CrossRef] [PubMed]
38. Yang, Q.; Jin, P.; Liu, B.; Zhao, L.; Cai, J.; Wei, Z.; Zuo, S.; Zhang, J.; Feng, L. Ultrafine carbon encapsulated NiRu alloys as bifunctional electrocatalysts for boosting overall water splitting: Morphological and electronic modulation through minor Ru alloying. *J. Mater. Chem. A* **2020**, *8*, 9049–9057. [CrossRef]
39. Kutyła, D.; Salcı, A.; Kwiecińska, A.; Kołczyk-Siedlecka, K.; Kowalik, R.; Żabiński, P.; Solmaz, R. Catalytic activity of electrodeposited ternary Co–Ni–Rh thin films for water splitting process. *Int. J. Hydrogen Energy* **2020**, *45*, 34805–34817. [CrossRef]
40. Skibińska, K.; Kutyła, D.; Yang, X.; Krause, L.; Marzec, M.M.; Żabiński, P. Rhodium-decorated nanoconical nickel electrode synthesis and characterization as an electrochemical active cathodic material for hydrogen production. *Appl. Surf. Sci.* **2022**, *592*, 153326. [CrossRef]
41. Nguyen, N.-A.; Choi, H.-S. Effect of Ni/Rh ratios on characteristics of NixRhy nanosponges towards high-performance hydrogen evolution reaction. *Data Br.* **2019**, *24*, 103941. [CrossRef] [PubMed]
42. Nguyen, N.-A.; Nguyen, V.-T.; Shin, S.; Choi, H.-S. NiRh nanosponges with highly efficient electrocatalytic performance for hydrogen evolution reaction. *J. Alloys Compd.* **2019**, *789*, 163–173. [CrossRef]
43. Zhang, C.; Liu, Y.; Chang, Y.; Lu, Y.; Zhao, S.; Xu, D.; Dai, Z.; Han, M.; Bao, J. Component-Controlled Synthesis of Necklace-Like Hollow Ni X Ru y Nanoalloys as Electrocatalysts for Hydrogen Evolution Reaction. *ACS Appl. Mater. Interfaces* **2017**, *9*, 17326–17336. [CrossRef] [PubMed]
44. Gomez, M.J.; Franceschini, E.A.; Lacconi, G.I. Ni and Ni x Co y Alloys Electrodeposited on Stainless Steel AISI 316L for Hydrogen Evolution Reaction. *Electrocatalysis* **2018**, *9*, 459–470. [CrossRef]
45. González-Buch, C.; Herraiz-Cardona, I.; Ortega, E.; García-Antón, J.; Pérez-Herranz, V. Synthesis and characterization of macroporous Ni, Co and Ni–Co electrocatalytic deposits for hydrogen evolution reaction in alkaline media. *Int. J. Hydrogen Energy* **2013**, *38*, 10157–10169. [CrossRef]
46. Lupi, C.; Dell'Era, A.; Pasquali, M. Nickel–cobalt electrodeposited alloys for hydrogen evolution in alkaline media. *Int. J. Hydrogen Energy* **2009**, *34*, 2101–2106. [CrossRef]
47. Vernickaite, E.; Tsyntsaru, N.; Sobczak, K.; Cesiulis, H. Electrodeposited tungsten-rich Ni-W, Co-W and Fe-W cathodes for efficient hydrogen evolution in alkaline medium. *Electrochim. Acta* **2019**, *318*, 597–606. [CrossRef]
48. Żabiński, P.; Mech, K.; Kowalik, R. Electrocatalytically active Co–W and Co–W–C alloys electrodeposited in a magnetic field. *Electrochim. Acta* **2013**, *104*, 542–548. [CrossRef]
49. Laszczyńska, A. Electrodeposited alloy electrodes in the Co–W–Mo system as highly efficient catalysts for hydrogen production from alkaline water electrolysis. *Mater. Chem. Phys.* **2024**, *314*, 128876. [CrossRef]
50. Laszczyńska, A.; Szczygieł, I. Electrocatalytic activity for the hydrogen evolution of the electrodeposited Co–Ni–Mo, Co–Ni and Co–Mo alloy coatings. *Int. J. Hydrogen Energy* **2020**, *45*, 508–520. [CrossRef]
51. Goranova, D.; Lefterova, E.; Rashkov, R. Electrocatalytic activity of Ni-Mo-Cu and Ni-Co-Cu alloys for hydrogen evolution reaction in alkaline medium. *Int. J. Hydrogen Energy* **2017**, *42*, 28777–28785. [CrossRef]
52. Negem, M.; Nady, H. Electroplated Ni-Cu nanocrystalline alloys and their electrocatalytic activity for hydrogen generation using alkaline solutions. *Int. J. Hydrogen Energy* **2017**, *42*, 28386–28396. [CrossRef]
53. Cui, X.; Xiao, P.; Wang, J.; Zhou, M.; Guo, W.; Yang, Y.; He, Y.; Wang, Z.; Yang, Y.; Zhang, Y.; et al. Highly Branched Metal Alloy Networks with Superior Activities for the Methanol Oxidation Reaction. *Angew. Chemie Int. Ed.* **2017**, *56*, 4488–4493. [CrossRef]
54. Koza, J.A.; Uhlemann, M.; Gebert, A.; Schultz, L. The effect of magnetic fields on the electrodeposition of CoFe alloys. *Electrochim. Acta* **2008**, *53*, 5344–5353. [CrossRef]
55. Huang, M.; Skibinska, K.; Zabinski, P.; Wojnicki, M.; Włoch, G.; Eckert, K.; Mutschke, G. On the prospects of magnetic-field-assisted electrodeposition of nano-structured ferromagnetic layers. *Electrochim. Acta* **2022**, *420*, 140422. [CrossRef]
56. Rode, S.; Henninot, C.; Matlosz, M. Complexation Chemistry in Nickel and Copper-Nickel Alloy Plating from Citrate Baths. *J. Electrochem. Soc.* **2005**, *152*, C248. [CrossRef]
57. Goranova, D.; Rashkov, R.; Avdeev, G.; Tonchev, V. Electrodeposition of Ni–Cu alloys at high current densities: Details of the elements distribution. *J. Mater. Sci.* **2016**, *51*, 8663–8673. [CrossRef]
58. Watanabe, T. Control of Macrostructure in Plated Films and Fabrication of Three-Dimensional Microstructure. In *Nano Plating—Microstructure Formation Theory of Plated Films and a Database of Plated Films*; Elsevier: Amsterdam, The Netherlands, 2004; pp. 195–205.
59. Landolt, D. Electrochemical and materials science aspects of alloy deposition. *Electrochim. Acta* **1994**, *39*, 1075–1090. [CrossRef]
60. Krause, L.; Skibińska, K.; Rox, H.; Baumann, R.; Marzec, M.M.; Yang, X.; Mutschke, G.; Żabiński, P.; Lasagni, A.F.; Eckert, K. Hydrogen Bubble Size Distribution on Nanostructured Ni Surfaces: Electrochemically Active Surface Area Versus Wettability. *ACS Appl. Mater. Interfaces* **2023**, *15*, 18290–18299. [CrossRef] [PubMed]
61. Elsharkawy, S.; Kutyła, D.; Zabinski, P. The Influence of the Magnetic Field on Ni Thin Film Preparation by Electrodeposition Method and Its Electrocatalytic Activity towards Hydrogen Evolution Reaction. *Coatings* **2023**, *13*, 1816. [CrossRef]

62. Solmaz, R.; Döner, A.; Kardaş, G. The stability of hydrogen evolution activity and corrosion behavior of NiCu coatings with long-term electrolysis in alkaline solution. *Int. J. Hydrog. Energy* **2009**, *34*, 2089–2094. [CrossRef]
63. Lee, J.M.; Bae, K.M.; Jung, K.K.; Jeong, J.H.; Ko, J.S. Creation of microstructured surfaces using Cu–Ni composite electrodeposition and their application to superhydrophobic surfaces. *Appl. Surf. Sci.* **2014**, *289*, 14–20. [CrossRef]
64. Eugénio, S.; Silva, T.M.; Carmezim, M.J.; Duarte, R.G.; Montemor, M.F. Electrodeposition and characterization of nickel–copper metallic foams for application as electrodes for supercapacitors. *J. Appl. Electrochem.* **2014**, *44*, 455–465. [CrossRef]
65. Mao, Y.-H.; Chen, C.-Y.; Fu, J.-X.; Lai, T.-Y.; Lu, F.-H.; Tsai, Y.-C. Electrodeposition of nickel-copper on titanium nitride for methanol electrooxidation. *Surf. Coat. Technol.* **2018**, *350*, 949–953. [CrossRef]